Current Biology 20, 62–68, January 12, 2010 ©2010 Elsevier Ltd All rights reserved DOI 10.1016/j.cub.2009.11.062

Report

# Sec24-Dependent Secretion Drives Cell-Autonomous Expansion of Tracheal Tubes in *Drosophila*

**Dominique Förster,[1,2] Kristina Armbruster,[1] and Stefan Luschnig[1,2,*]**
[1]Institute of Zoology
[2]PhD Program in Molecular Life Sciences
Universität Zürich, CH-8057 Zürich, Switzerland

## Summary

**Epithelial tubes in developing organs, such as mammalian lungs and insect tracheae, need to expand their initially narrow lumina to attain their final, functional dimensions [1]. Despite its critical role for organ function, the cellular mechanism of tube expansion remains unclear. Tracheal tube expansion in *Drosophila* involves apical secretion and deposition of a luminal matrix [2–5], but the mechanistic role of secretion and the nature of forces involved in the process were not previously clear. Here we address the roles of cell-intrinsic and extrinsic processes in tracheal tube expansion. We identify mutations in the *sec24* gene *stenosis*, encoding a cargo-binding subunit of the COPII complex [6–8]. Via genetic-mosaic analyses, we show that *stenosis*-dependent secretion drives tube expansion in a cell-autonomous fashion. Strikingly, single cells autonomously adjust both tube diameter and length by implementing a sequence of events including apical membrane growth, cell flattening, and taenidial cuticle formation. Known luminal components are not required for this process. Thus, a cell-intrinsic program, rather than nonautonomous extrinsic cues, controls the dimensions of tracheal tubes. These results indicate a critical role of membrane-associated proteins in the process and imply a mechanism that coordinates autonomous behaviors of individual cells within epithelial structures.**

## Results and Discussion

We used the *Drosophila* tracheal system [9–11] to dissect the cellular mechanism of epithelial tube expansion. Tracheal cells secrete a matrix consisting of proteins and chitin into the expanding lumen [5, 12, 13]. It was proposed that the luminal matrix could provide forces that drive the expansion process [4, 5, 14]. However, the role of matrix secretion and the nature of the relevant secreted molecules have not been clear. Here we address the mechanistic role of secretion in tracheal tube expansion.

### *stenosis* Is Required for Tracheal Tube Dilation and Secretion

In a mutagenesis screen for genes controlling tracheal morphogenesis and secretion, we identified a complementation group defective in tracheal tube dilation (Figures 1A and 1B). Based on the narrow lumen phenotype of the mutants, we named the locus *stenosis* (*sten*). In addition to the tube dilation defect, Vermiform-RFP (Verm-RFP), which is secreted into the tracheal lumen in wild-type embryos, was partially retained in *sten* mutant tracheal cells (Figures 1A and 1B), where it colocalized with the endoplasmic reticulum (ER; data not shown), suggesting that *sten* is required for ER export of Verm-RFP. Similar to Verm-RFP, endogenous Verm protein was partially retained intracellularly (Figures 1D and 1G). Moreover, both apical (Stranded at second [Sas]; Figures 1E and 1H) and basolateral (basigin-GFP; data not shown) transmembrane (TM) proteins were affected, suggesting that *sten* is required for general secretion. However, luminal localization of chitin was not impaired (see Figure S5 available online). We conclude that *sten* is required for tracheal tube dilation and for protein secretion.

### *sten* Mutations Affect Secretion, but Not Polarity, in Embryonic Epithelia

*sten* embryos also showed defects in other epithelia, including a lack of epidermal cuticle, aberrant epidermal cell shapes, and dorsal closure defects (see Figure S1). However, apicobasal cell polarity was apparently not affected, because apical (E-cadherin [E-Cad], Crumbs [Crb], Bazooka-GFP; Figures 1K and 1L; Figure S5; data not shown) as well as basolateral (Coracle [Cora], Fasciclin III [FasIII], Discs large-GFP; Figures S1 and S4; data not shown) proteins localized correctly in *sten* mutant epidermal and tracheal cells. Moreover, *sten* mutant epithelia contained basolateral septate junctions (Figures 1P and 1R). These results suggest that epithelial polarity is maintained despite the secretion defects in *sten* embryos.

### *sten* Encodes a Sec24 Family Protein

All three *sten* alleles contain point mutations in the previously uncharacterized gene CG10882 (Figure 2A; Figure S2). CG10882 encodes a protein related to the Sec24 subunit of COPII (*co*at *p*rotein complex II) vesicles, which transport cargo from the ER to the Golgi apparatus (Figure 2B; [6–8]). All three *sten* alleles encode C-terminally truncated proteins, which are presumed to be incapable of complex formation with Sec23 and should consequently lack any function in COPII trafficking [15]. Tracheal phenotypes of $sten^{G200}$ and $sten^{H24}$ homozygotes were indistinguishable from embryos carrying these mutations in *trans* to a *sten* deletion (*Df(2L)Exel7010*; Figures 1G–1I; data not shown), corroborating that these alleles are strong loss-of-function mutations. Finally, tracheal-specific expression of either untagged or N-terminally GFP-tagged CG10882 protein fully rescued the tube dilation and secretion defects of *sten* mutants, indicating that these defects are due to a requirement of CG10882 in tracheal cells (Figures 1A–1C and 1J). Consistent with these findings, CG10882 mRNA was expressed in embryonic epithelia, with elevated levels in tracheal cells (data not shown). Maternal CG10882 mRNA was present in early embryos, suggesting that the late onset of the defects in zygotic *sten* mutants is due to perduring maternal *sten* gene products. Consistent with this view, maternal *sten* function was essential for cell viability (data not shown). We conclude that *sten* encodes a Sec24-related protein that is required in tracheal cells for tube dilation and

*Correspondence: stefan.luschnig@zool.uzh.ch

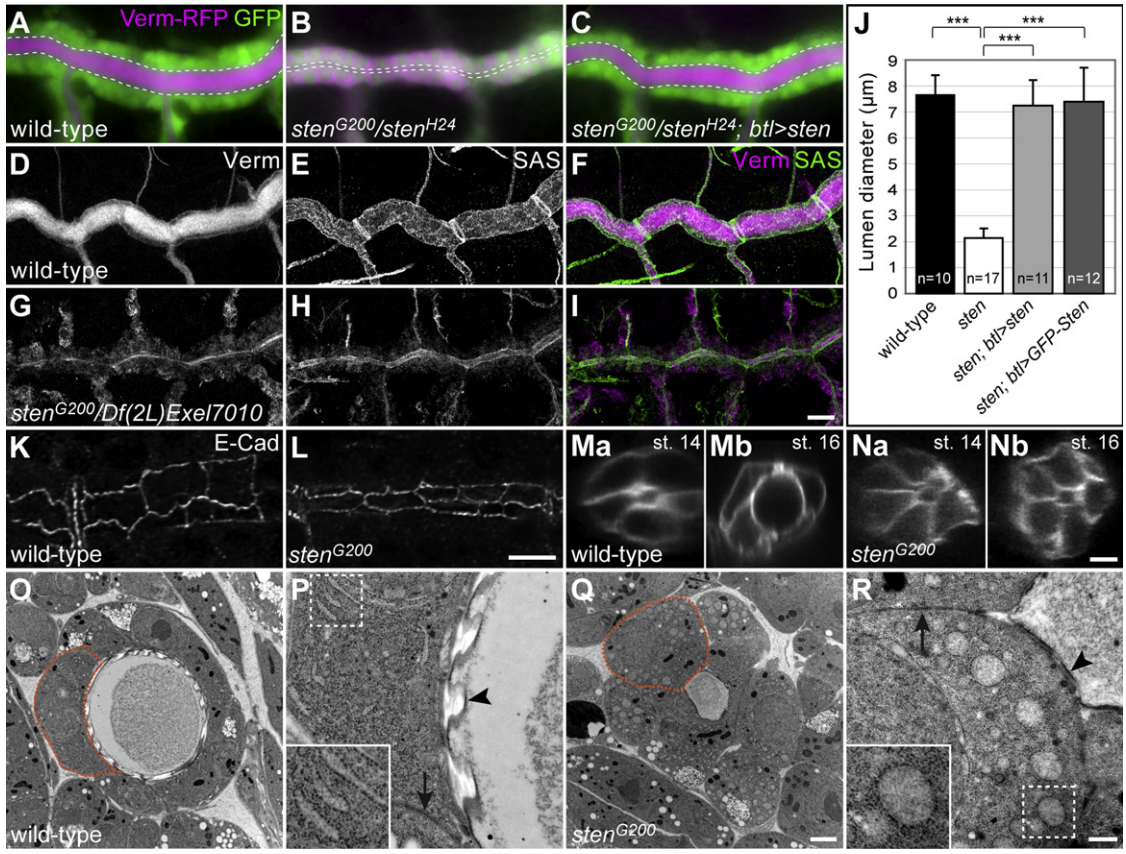


Figure 1. Effects of *stenosis* Mutations on Secretion, Tracheal Tube Expansion, and Tracheal Cell Morphology

(A–C) Wide-field fluorescence images of living embryos expressing GFP (green) and Vermiform-RFP (Verm-RFP) (magenta) in tracheal cells under the control of *btl*-Gal4. Verm-RFP is secreted into the tracheal lumen in wild-type embryos (A) but accumulates in tracheal cells in *sten* mutants (B). The dorsal trunk (DT) lumen (dashed lines) is dilated in stage 16 wild-type embryos (A) but remains narrow in *sten* mutants (B). Verm-RFP secretion and lumen dilation are fully restored by tracheal-specific expression of *sten* (C).

(D–I) Confocal projections of stage 16 wild-type (D–F) and *sten* mutant embryos (G–I) stained for Verm (D and G) and Sas (E and H) proteins. Verm and Sas accumulate in the lumen and at the apical membrane, respectively, in the wild-type, but are partially retained in tracheal cells in *sten* embryos.

(J) Quantification of luminal diameter in DT metamere 6. Tube diameter is significantly reduced in $sten^{G200}/sten^{H24}$ mutants but is fully rescued by *btl-Gal4*-driven tracheal-specific expression of *sten* or *GFP-Sten*, as indicated by Student's t test (***$p < 0.001$). Tube diameter is not significantly different between wild-type and rescued embryos ($p > 0.1$). Error bars represent mean ± standard deviation.

(K and L) Confocal projections of DT in stage 16 wild-type (K) and *sten* mutant (L) embryos stained for E-cadherin (E-Cad). The apical perimeter of tracheal cells is small in *sten* mutants compared to the wild-type. Note that apical E-Cad localization is not affected in *sten* mutants.

(Ma–Nb) Cross sections of posterior DT tubes in living wild-type (Ma and Mb) and *sten* mutant (Na and Nb) embryos at stage 14 and stage 16. Tracheal cells express Src-GFP to label cell membranes. Note that cell profiles in the wild-type change from conical at stage 14 to flattened-cuboidal at stage 16, whereas *sten* mutant cells stay conical.

(O–R) Abnormal tracheal cell shapes and endoplasmic reticulum (ER) structure in *sten* mutants. Transmission electron microscopy (TEM) cross sections of posterior DT in stage 16 embryos are shown. The outline of one tracheal cell is marked by an orange dotted line in (O) and (Q). Wild-type tracheal cells are flat and cuboidal (O) and show cuticular taenidia on the luminal surface (arrowhead in P). Matrix material (dark gray oval inside lumen in O) is being cleared, as indicated by a crescent-shaped gap between the luminal surface and the remaining matrix. The rough ER is organized in flat, regular cisternae (P). *sten* tracheal cells show conical profiles with a small, convex apical surface lacking cuticle, and the entire lumen is filled with matrix material (Q and R). The ER lumen is dramatically enlarged (R). Note that *sten* mutants still show basolateral septate junctions (arrows in P and R) and the electron-dense cuticular envelope (arrowheads in P and R). Also note indentations of the luminal surface at cell borders in *sten* mutants (R). Insets in (P) and (R) are close ups of boxed regions marked by dashed lines.

Scale bars represent 10 μm (A–I), 5 μm (K–Nb), 2 μm (O and Q), and 0.5 μm (P and R). See also Figure S1.

protein secretion. Similar roles were previously reported for other COPII components (Sar1, Sec13, Sec23; [5]).

### GFP-Sten Protein Localizes to ER Exit Sites

To analyze the subcellular localization of Sten, we generated a GFP-Sten fusion protein. GFP-Sten accumulated at punctate structures in tracheal cells, with an average of 12.2 ± 2.8 (n = 22) punctae per cell (Figure 2F). These punctae were embedded within the ER and colocalized with the COPII marker Sec31-RFP and the ER exit site (ERES) protein Sec16 (Figures 2C–2I; [6, 16]), suggesting that GFP-Sten accumulates at ERES. Consistent with these findings, Sec31-RFP-labeled punctae localized adjacent to, but nonoverlapping with, the *trans*-Golgi marker galactosyltransferase-GFP (GalT-GFP; Figure 2J; [17]). Interestingly, the morphology and number of Sec31-RFP-labeled punctae did not change in *sten* mutants (12.3 ± 3.6 punctae per cell; n = 22) despite dramatic effects on Golgi localization of GalT-GFP (Figure 2K) and on ER morphology (Figure 1R) in *sten* mutant cells, suggesting that ER exit sites are maintained in the absence of *sten* function.

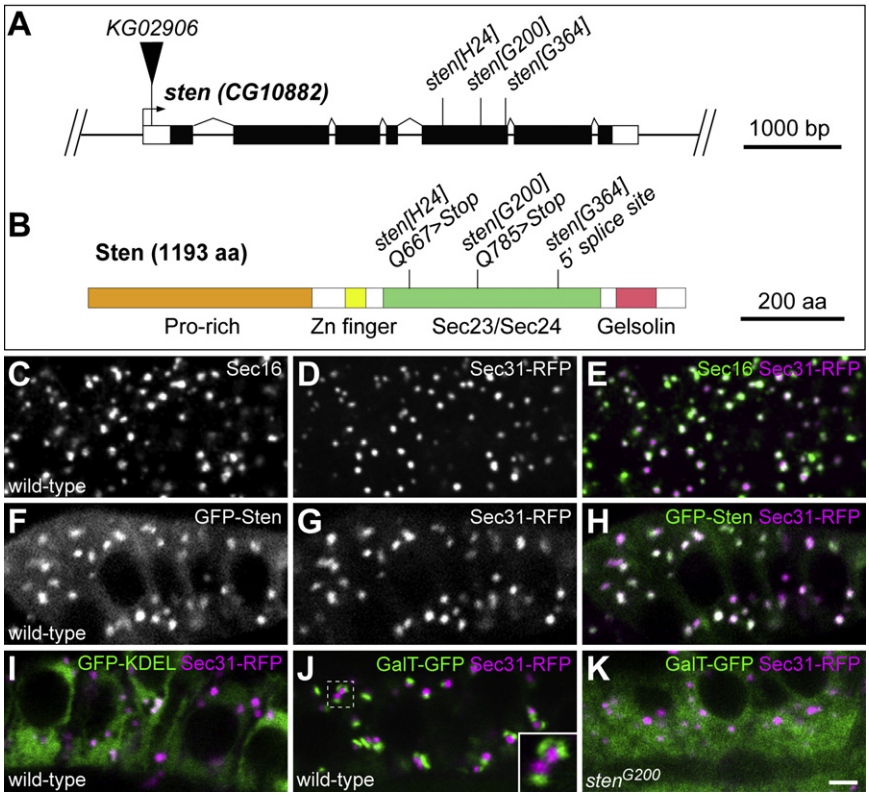


Figure 2. *stenosis* Encodes a Sec24 Protein that Localizes at ER Exit Sites

(A) Structure of the *stenosis* gene. A single transcript is annotated in FlyBase. Exons are shown as boxes with coding regions filled in black. The $sten^{G200}$ and $sten^{H24}$ alleles contain premature translation termination codons within the Sec23/Sec24 trunk domain, which forms the interface between Sec23 and Sec24 in the COPII complex [15]. $sten^{G364}$ contains a splice site mutation resulting in retention of intron 5 in the mRNA. The mutant transcripts were detectable by semiquantitative reverse transcriptase-polymerase chain reaction (Figure S2). A *P* element, *KG02906* (black triangle), inserted in the 5′ untranslated region is allelic to *sten* mutations. The *Drosophila melanogaster* genome contains a second Sec24 homolog referred to as *sec24* (CG1472; FlyBase). Unlike *sten*, zygotic *sec24* function is not essential during embryogenesis (data not shown).

(B) Domain organization of the Sten protein. Size of the protein in amino acids (aa) and mutations in the *sten* alleles are indicated. The proline-rich domain, zinc finger, Sec23/Sec24 trunk domain, and gelsolin-homology region are highlighted by colored boxes.

(C–K) Localization of GFP-Sten protein at ER exit sites. Confocal sections of tracheal DT cells in fixed (C–E) or living (F–K) stage 15 embryos are shown. Fluorescent proteins were expressed in tracheal cells with *btl-Gal4*.

(C–E) Sec31-RFP (D) localizes at punctate structures labeled by the ER exit site (ERES) protein Sec16 (C). Note that every dot labeled by Sec31-RFP (magenta in E) is also labeled by Sec16 (green in E), even though relative signal intensities of Sec31-RFP and Sec16 vary.

(F–H) GFP-Sten (F) accumulates in punctate structures that colocalize with Sec31-RFP (G). The merge is shown in (H).

(I) Sec31-RFP punctae (magenta) are embedded in the ER labeled by GFP-KDEL (green).

(J) Sec31-RFP (magenta) localizes in close proximity to, but nonoverlapping with, the *trans*-Golgi marker GalT-GFP (green). Inset shows close up of boxed region marked by a dashed line.

(K) Punctate localization of Sec31-RFP (magenta) is maintained in *sten* mutants, although Golgi localization of GalT-GFP (green) is lost (compare green signals in K to J).

Scale bar in (C)–(K) represents 2 μm. See also Figure S2.

Taken together, these results indicate that Sten localizes at ERES, consistent with a function in ER export and COPII trafficking.

### *sten* Is Required for Cell Shape Changes during Tracheal Tube Dilation

We noticed that tracheal dorsal trunk (DT) cells in stage 16 *sten* mutants occupied a smaller luminal surface area outlined by apical E-Cad or lateral Cora staining compared to wild-type controls (Figures 1K and 1L; Figure S4). Correspondingly, transmission electron microscopy (TEM) analysis revealed flattened cuboidal shapes of DT cells in the wild-type, whereas DT cells in *sten* embryos had conical profiles with a small apical surface (Figures 1O and 1Q). The shapes of *sten* mutant cells were reminiscent of wild-type tracheal cells at the onset of tube expansion, suggesting that *sten* mutants do not undergo the normal program of cell shape changes during tube expansion (Figures 1M and 1N). Instead of the smooth luminal surface in the wild-type, apical cell surfaces in *sten* mutants were convex toward the lumen and the luminal surface was indented at cell borders (Figures 1P and 1R). In addition, *sten* mutants lacked cuticular taenidia and failed to clear matrix material from the lumen. Moreover, the rough ER appeared dramatically bloated compared to the flat ER cisternae in the wild-type (Figures 1P and 1R). These phenotypes are qualitatively similar to but more severe than those described for *sar1* mutants [5]. We conclude that *sten*-dependent secretion is required for ER organization, taenidia formation, and cell shape changes during tracheal tube expansion.

### Secretory Activity Acts Locally in Tube Expansion

To dissect the mechanistic role of *sten*-dependent secretion in tube expansion, we asked whether secretion acts in a cell-intrinsic fashion or via extrinsic cues. It was proposed that secretion-dependent extrinsic cues, e.g., luminal pressure as a consequence of matrix deposition or ion transport, could drive tracheal tube dilation [4, 5, 14], implying a nonautonomous role of secretion in the process. To ask whether locally restricted secretory activity can drive tube dilation nonautonomously in distant parts of the tube, we used *Abdominal B* (*Abd-B*)-Gal4 [18] to express GFP-Sten in cells of parasegment 13, including the posteriormost tracheal metamere (Tr10; Figure 3F; Figure S3). We then analyzed *sten* mutant embryos in which *sten* function was restored in Tr10. Strikingly, tracheal tube dilation was rescued in all branches of Tr10, whereas the rest of the tracheal system showed no signs of restored tube dimensions or morphology (Figures 3C and 3D). At stage 17, tubes in Tr10 showed expanded diameter, cuticular taenidia, and partially restored Verm secretion, whereas tubes anterior

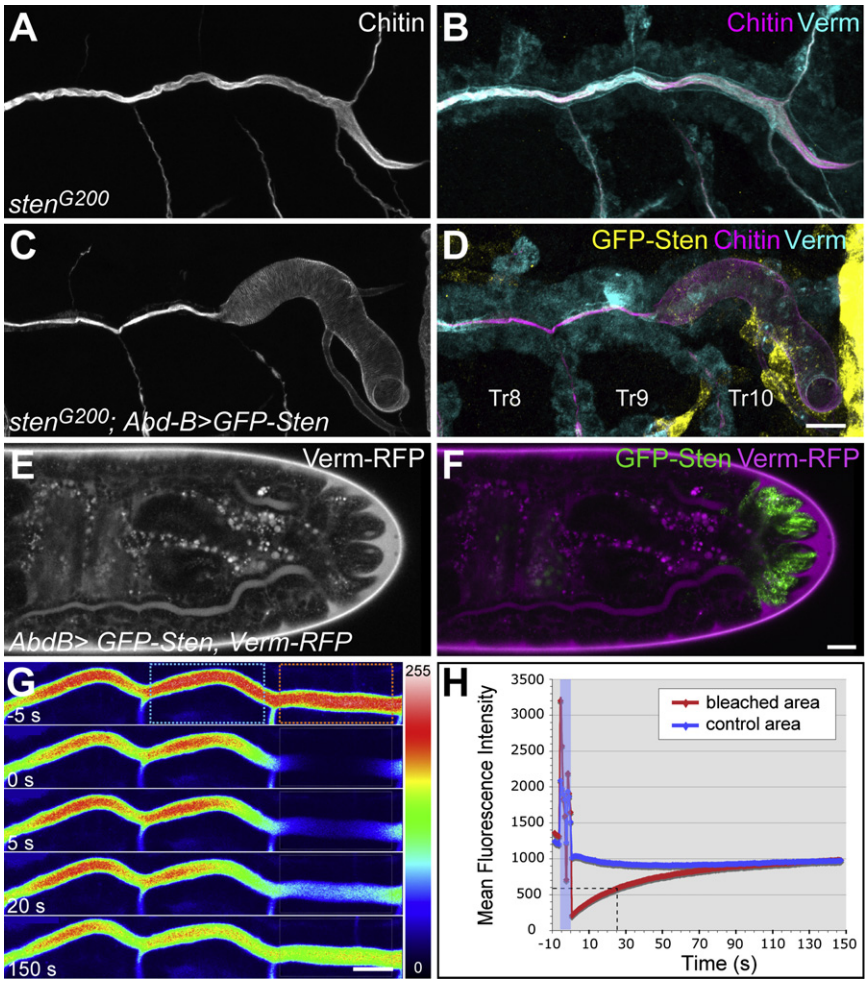


Figure 3. Secretory Activity Acts Locally to Drive Tube Expansion

(A–D) Confocal projections of tracheal metameres 8–10 in stage 16 *sten* mutant embryos stained for chitin, Verm, and GFP. Expression of GFP-Sten in Tr10 locally rescues tracheal tube dilation, taenidia formation, and Verm secretion exclusively in Tr10 (compare B and D). Note that *Abd-B*-Gal4-driven GFP-Sten expression ceases in older embryos; thus, GFP-Sten (yellow in D) is no longer detectable in all cells of Tr10 at stage 16.

(E and F) Confocal section of a living wild-type embryo expressing Verm-RFP (magenta in F) and GFP-Sten (green in F) under the control of *Abd-B*-Gal4. Verm-RFP is exclusively expressed by the GFP-labeled cells in parasegment (PS) 13, including the last tracheal metamere. Note that Verm-RFP is distributed throughout the entire tracheal lumen. Verm-RFP at the periphery of the embryo presumably originates from GFP-Sten-expressing epidermal cells in PS13.

(G and H) Secreted proteins diffuse rapidly inside the tracheal lumen. Serp-CBD-GFP was expressed in tracheal cells with *btl*-Gal4. The protein accumulates inside the lumen (G). The region marked by an orange box in DT metamere 7 was bleached for 6 s, and fluorescence recovery was measured. Selected frames from a representative experiment in a stage 15 wild-type embryo are shown (see Movie S1). Fluorescence rapidly recovers by influx of Serp-CBD-GFP from both sides flanking the bleached region. Time is indicated at lower left. Signal intensities are indicated by a heat map shown at right.

(H) Analysis of fluorescence recovery after photobleaching (FRAP) experiment shown in (G). Average signal intensities in the bleached region (orange box in G) and in control regions (blue box in G) were plotted. The recovery half-time (dashed line) is 25.1 s. Independent FRAP experiments revealed similar results (n = 5; data not shown). Figure S3 shows a corresponding FRAP experiment in a *sten* mutant embryo.

Scale bars represent 10 μm (A–D), 25 μm (E and F), and 10 μm (G). See also Figure S3.

to Tr10 were narrow, lacked taenidia, and showed high levels of retained Verm. Importantly, there was a sharp border between these phenotypes at the fusion joint between Tr9 and Tr10, suggesting that the rescuing activity does not spread away from the GFP-Sten-expressing cells. These results suggest that local secretion-dependent events drive the tube dilation process.

### Secreted Proteins Rapidly Diffuse in the Tracheal Lumen

The local effect observed in the previous experiment suggests that the *sten*-dependent activity that mediates tube dilation is not diffusible. This could be due to membrane localization of the relevant proteins or, alternatively, to impaired diffusion of secreted proteins in the matrix-filled lumen. To ask whether proteins are capable of diffusing within the tracheal lumen, we generated embryos coexpressing Verm-RFP and GFP-Sten in Tr10 under the control of *Abd-B*-Gal4 (Figures 3E and 3F). In these embryos, Verm-RFP was detectable throughout the entire DT lumen, suggesting that the protein diffuses in the luminal space. Importantly, a similar distribution of Verm-RFP was observed in *sten* embryos expressing Verm-RFP and GFP-Sten in Tr10, suggesting that luminal protein mobility is maintained in *sten* mutants (Figure S3). Moreover, we directly measured the mobility of a secreted GFP fusion protein, Serp-CBD-GFP, in the tracheal lumen via fluorescence recovery after photobleaching (FRAP) experiments (Figures 3G and 3H; Movies S1 and S2). Upon bleaching of one DT metamere, fluorescence in the lumen recovered rapidly by diffusion from both sides flanking the bleached area (Figure 3G). Remarkably, recovery kinetics were similar in wild-type and *sten* embryos, with half-maximal recovery times of approximately 25 s (Figure 3H; Figure S3), indicating that proteins can diffuse rapidly within the lumen and that mobility is not significantly impaired by the narrow tubes in *sten* mutants. We conclude that despite the high mobility of secreted proteins in the lumen, secretion acts locally to mediate tracheal tube expansion.

### Tracheal Cells Individually Dilate the Lumen by Expanding Their Apical Surface

Although our findings described above point to a cell-autonomous function of secretion in tube dilation, it is not clear whether a contiguous group of secreting cells is required to implement tube dilation, or whether a single cell is able to dilate the lumen autonomously. To address this point, we generated *sten* embryos bearing individual GFP-Sten-expressing cells

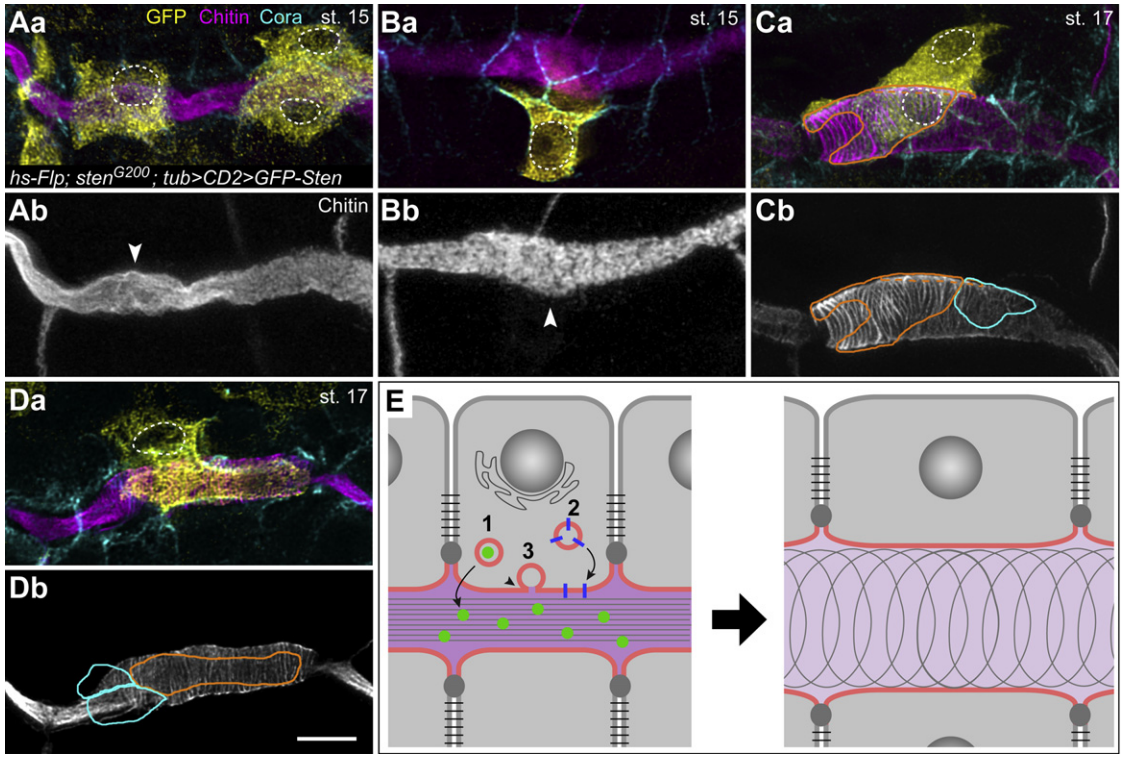


Figure 4. Individual Tracheal Cells Autonomously Expand the Lumen by Enlarging Their Apical Membrane

(Aa–Db) Mosaic analysis to test autonomy of *sten* function. GFP-Sten expression was induced in random individual cells in *sten* mutant embryos of the genotype *hs-Flp/+; sten$^{G200}$/sten$^{G200}$; tub > CD2 > Gal4 UAS-GFP/UAS-GFP-Sten*. Confocal projections of embryos stained for GFP (yellow), chitin (magenta), and Cora (cyan) are shown. Positions of nuclei stained by Hoechst (data not shown) are outlined by dashed white lines. (Ab)–(Db) show the chitin channel of corresponding merged images in (Aa)–(Da). At stage 15, the luminal surface of rescued cells is bulging out (arrowheads in Ab and Bb). At stage 17, the apical surface (demarcated by Cora staining) is dramatically enlarged in rescued cells (orange outline in Cb and Db) compared to neighboring mutant cells (cyan outline in Cb and Db), and rescued cells display taenidial rings on the luminal surface. Note that rescued cells expand autonomously in diameter and in length. A 3D animation of the two labeled cells in (Ca) is shown in Movie S3. Additional examples of rescued cells are shown in Figure S4.

(E) Model summarizing roles of secretion in tracheal tube expansion. *sten*-dependent trafficking deposits soluble secreted proteins (1) in the lumen and inserts membrane proteins (2) and membrane material (3) into the apical cell surface. The cell-autonomous function of *sten* in tube expansion suggests a critical role of membrane material and/or membrane proteins, but not of soluble secreted proteins, in the lumen. See text for details.

Scale bar represents 5 μm. See also Figures S4 and S5.

(Figure 4). Secretory function was rescued in these cells, as indicated by restored Verm secretion (data not shown). Strikingly, the rescued DT cells dramatically expanded their luminal surface area, both diametrically and longitudinally, relative to neighboring mutant cells, which showed no signs of expansion (Figures 4Aa–4Db; Figure S4; n = 17). The rescued cells were hat shaped with conspicuous apical processes along the lumen (Figures 4Ba–4Db). These cells occupied up to four times more luminal surface compared to neighboring mutant cells, as indicated by Cora staining outlining cell borders. This effect was also observed in other tracheal cell types besides DT cells and is not due to GFP-Sten overexpression, because cells expressing GFP-Sten in wild-type embryos did not show excessive expansion (Figure S4). The luminal surface underlying rescued cells showed characteristic bulges, suggesting that restored secretion in a single cell leads to local luminal dilation (Figures 4A and 4B). This effect was apparent at stage 15, prior to the formation of tracheal cuticle. At stage 17, taenidial rings were visible on the luminal surface of GFP-Sten-expressing cells. Interestingly, taenidia extended around the entire lumen (encompassing the surface of mutant cells) and up to one cell diameter away from a rescued cell onto the surface of adjacent mutant cells (Figures 4C and 4D; Figure S4; Movie S3). The presence of taenidia correlated with local dilation of the lumen. These findings suggest that cuticle synthesized by a rescued cell spreads over a short range and thereby slightly extends the local dilation. Taken together, our results indicate that tracheal tube expansion is driven largely by a cell-intrinsic secretion-dependent morphogenetic program rather than by extrinsic cues. Strikingly, a single cell autonomously executes all steps of this program, which includes apical membrane growth, diametric and longitudinal expansion, and taenidia formation.

As previously proposed [5], two principle scenarios for the role of secretion in epithelial tube expansion are conceivable (Figure 4E). In the first scenario, secretion acts nonautonomously by inducing mechanical or chemical changes in the lumen that in turn impinge on epithelial cells. For instance, ion-transport-dependent fluid accumulation is required for expansion and coalescence of nascent lumens in the zebrafish gut [19]. In developing mammalian lungs, chloride-transport-dependent hydrostatic pressure was proposed to maintain and dilate the lumen and to stimulate growth by signaling via stretch sensors [20]. However, the nature of the presumed stretch-sensing pathway is not known. In the second scenario, secretion acts autonomously through cell-intrinsic events that

modulate cell shape, e.g., polarized delivery of membrane and proteins to the cell surface. We demonstrate here that tracheal tube expansion is a cell-autonomous process driven largely by cell-intrinsic forces. Extrinsic cues emanating from the lumen are not required to initiate or to propel the expansion process. Three lines of evidence support these conclusions. First, none of the known luminal components, including secreted proteins and chitin, are required for tracheal tube expansion. Conversely, lack of luminal proteins or of chitin causes elongated or overdilated tubes, respectively, suggesting that the luminal matrix restricts tube expansion rather than promoting it [12, 13, 21, 22]. Moreover, lack of a functional epithelial barrier does not impair tube dilation [23], indicating that presumptive luminal pressure is not required. Second, despite rapid diffusion of secreted proteins, secretion acts locally to promote tube dilation, suggesting that a cell-autonomous aspect of secretion is driving tube expansion. Third and most striking, a single cell is able to autonomously execute a program of cell shape changes that result in local expansion of the lumen. This indicates that any essential activities involved in this program are cell intrinsic. Thus, either the molecules mediating these activities are secreted but only act at a short range or, alternatively, the relevant secretory cargo is associated with the plasma membrane (Figure 4E). Selective apical membrane growth and remodeling was shown to play a key role in epithelial tube expansion [2, 24, 25]. Candidates for proteins that could mediate *sten*-dependent apical expansion include the TM protein Crb, which determines apical membrane size in a dose-dependent fashion and is involved in tube morphogenesis [25–27]. Indeed, we found that overexpression of Crb caused overdilation of the tracheal lumen in a *sten*-dependent manner (Figure S5). However, localization and levels of endogenous Crb protein appeared normal in *sten* mutants, presumably because maternal *sten* function was sufficient for Crb secretion. Thus, Crb is unlikely to be a main effector of *sten*-dependent secretion in tube dilation. Alternatively, exocytosis may directly modulate apical surface area by polarized delivery and insertion of membrane material at the apical side. An actin/myosin-dependent apical membrane trafficking pathway in tracheal cells was recently described [28]. It will be crucial to characterize the vesicles that mediate *sten*-dependent apical expansion.

Importantly, the autonomous expansive behavior of individual cells must be tightly coordinated to ensure uniform expansion of the epithelium. Because tracheal tube diameter is constant despite local variations in the number of cells surrounding the lumen, cells must exchange information about the relative surface area that they occupy. What coordinates and limits the intrinsic tendency of epithelial cells to expand their surface? We propose that apical expansion is controlled by interactions of cells with the luminal matrix, which acts as a scaffold that integrates forces along the tube. Contact with the luminal matrix appears to limit apical membrane growth during tube expansion, whereas at later stages rigid cuticle physically stabilizes the apical surface. Accordingly, luminal matrix defects result in dramatic overexpansion of tracheal cells [12, 13, 21, 22].

Our findings could have implications for the mechanisms of tube expansion in other organs and organisms. Intriguingly, renal cyst formation in a polycystic kidney disease (PKD) mouse model is a focal process initiated by clonal expansion of individual cells that become homozygous for a *Pkd2* mutation [29]. Polycystins, TM proteins on the surface of apical cilia, were proposed to function as mechanical sensors in cell-matrix interactions [1]. It is tempting to speculate that cell-autonomous regulation of apical membrane size may be involved in controlling renal tubule diameter in an analogous fashion to what we have described for tracheal tubes.

## Experimental Procedures

### Isolation of *sten* Mutations

The mutagenesis screen will be described in detail elsewhere. In brief, mutations were induced by ethyl methanesulfonate feeding of males carrying a *btl-Gal4 UAS-GFP UAS-Verm-RFP* chromosome. $F_2$ lines were established, and living $F_3$ embryos were scored for tracheal morphology and for Verm-RFP secretion. The *sten* locus was mapped to the cytological interval 22D4-22E1 by noncomplementation of *Df(2L)BSC37*, *Df(2L)Exel6007*, and *Df(2L)Exel7010* (FlyBase). The *CG10882* coding sequence, including exon-intron boundaries, was amplified by polymerase chain reaction (PCR) from homozygous *sten* embryos and from the parental strain. PCR products were sequenced on both strands. The point mutations in $sten^{G200}$, $sten^{G364}$, and $sten^{H24}$ alleles reside in exon 5 and were revealed by sequencing with oligonucleotides CG10882-5F (5′-GAATGAAAATTTGTCTCGGTTG) and CG10882-6R (5′-GCTGCACGAGGTGTACAAGA).

### Genetic Mosaic Experiments

Individual GFP-Sten-expressing cells in *sten* embryos were generated with the flip-out technique [30] and a *tub* > *CD2* > *Gal4* transgene. Females carrying *hs-Flp*$^{122}$*; sten*$^{G200}$*/CyO Dfd-YFP; tub* > *CD2* > *Gal4 UAS-GFP* were crossed to males carrying *sten*$^{G200}$*/CyO Dfd-YFP; UAS-GFP-Sten*. Embryos (2–5 hr old) from this cross were subjected to an 8 min heat shock at 37°C. Embryos were allowed to develop at 24°C before they were fixed at 15–18 hr after egg lay. GFP-Sten-expressing cells were visualized by anti-GFP antibody staining.

### Antibodies and Immunostainings

The following primary antibodies were used: rabbit anti-Verm (1:300; [21]), guinea pig anti-Verm (1:500; [22]), mouse anti-GFP (1:500; Clontech), rabbit anti-GFP (1:500; gift from S. Heidmann), guinea pig anti-Cora (1:200; [31]), mouse anti-Crb (1:50; Developmental Studies Hybridoma Bank [DSHB]), rat anti-E-Cad (1:100; DSHB), rabbit anti-Sas (1:250; gift from D. Cavener; unpublished data; [32]), mouse anti-FasIII (1:50; DSHB), rabbit anti-Sec16 (1:1000; [16]). Rhodamine- or fluorescein isothiocyanate (FITC)-conjugated chitin-binding probe (1:100; New England Biolabs) was used to detect chitin. Hoechst 33258 was used to detect DNA. Secondary antibodies were conjugated with Alexa 488, Alexa 568 (Molecular Probes), or Cy5 (Jackson ImmunoResearch). Embryos were fixed in 4% formaldehyde for 20 min or were heat fixed (for anti-Sec16 stainings) and were devitellinized by shaking in methanol/heptane or in ethanol/heptane (for anti-E-Cad stainings).

### Supplemental Information

Supplemental Information includes Supplemental Experimental Procedures, five figures, and three movies and can be found with this article online at doi:10.1016/j.cub.2009.11.062.

### Acknowledgments

We thank S. Limmer for help in the screen; G. Barmettler, A. Kaech, and U. Ziegler for help with TEM; and M. Affolter, K. Basler, R. Fehon, E. Knust, M. Krasnow, C. Rabouille, C. Samakovlis, E. Sanchez-Herrero, and R. Yagi for antibodies and fly stocks. We thank R. Metzger, M. Metzstein, F. Schnorrer, and A. Spang for comments on the manuscript. We are grateful to C. Lehner for support and discussions. This work was supported by the Swiss National Science Foundation, the German Research Foundation, the Julius Klaus-Stiftung Zürich, and the Kanton Zürich. D.F. is supported by a Müller fellowship of the Zürich PhD program in Molecular Life Sciences.

Received: October 7, 2009
Revised: November 13, 2009
Accepted: November 17, 2009
Published online: December 31, 2009

**References**

1. Lubarsky, B., and Krasnow, M.A. (2003). Tube morphogenesis: Making and shaping biological tubes. Cell *112*, 19–28.
2. Beitel, G.J., and Krasnow, M.A. (2000). Genetic control of epithelial tube size in the *Drosophila* tracheal system. Development *127*, 3271–3282.
3. Grieder, N.C., Caussinus, E., Parker, D.S., Cadigan, K., Affolter, M., and Luschnig, S. (2008). gammaCOP is required for apical protein secretion and epithelial morphogenesis in *Drosophila melanogaster*. PLoS ONE *3*, e3241.
4. Jayaram, S.A., Senti, K.A., Tiklová, K., Tsarouhas, V., Hemphälä, J., and Samakovlis, C. (2008). COPI vesicle transport is a common requirement for tube expansion in Drosophila. PLoS ONE *3*, e1964.
5. Tsarouhas, V., Senti, K.A., Jayaram, S.A., Tiklová, K., Hemphälä, J., Adler, J., and Samakovlis, C. (2007). Sequential pulses of apical epithelial secretion and endocytosis drive airway maturation in *Drosophila*. Dev. Cell *13*, 214–225.
6. Mancias, J.D., and Goldberg, J. (2005). Exiting the endoplasmic reticulum. Traffic *6*, 278–285.
7. Matsuoka, K., Orci, L., Amherdt, M., Bednarek, S.Y., Hamamoto, S., Schekman, R., and Yeung, T. (1998). COPII-coated vesicle formation reconstituted with purified coat proteins and chemically defined liposomes. Cell *93*, 263–275.
8. Pagano, A., Letourneur, F., Garcia-Estefania, D., Carpentier, J.L., Orci, L., and Paccaud, J.P. (1999). Sec24 proteins and sorting at the endoplasmic reticulum. J. Biol. Chem. *274*, 7833–7840.
9. Affolter, M., and Caussinus, E. (2008). Tracheal branching morphogenesis in *Drosophila*: New insights into cell behaviour and organ architecture. Development *135*, 2055–2064.
10. Ghabrial, A., Luschnig, S., Metzstein, M.M., and Krasnow, M.A. (2003). Branching morphogenesis of the *Drosophila* tracheal system. Annu. Rev. Cell Dev. Biol. *19*, 623–647.
11. Uv, A., Cantera, R., and Samakovlis, C. (2003). *Drosophila* tracheal morphogenesis: Intricate cellular solutions to basic plumbing problems. Trends Cell Biol. *13*, 301–309.
12. Devine, W.P., Lubarsky, B., Shaw, K., Luschnig, S., Messina, L., and Krasnow, M.A. (2005). Requirement for chitin biosynthesis in epithelial tube morphogenesis. Proc. Natl. Acad. Sci. USA *102*, 17014–17019.
13. Tonning, A., Hemphälä, J., Tång, E., Nannmark, U., Samakovlis, C., and Uv, A. (2005). A transient luminal chitinous matrix is required to model epithelial tube diameter in the *Drosophila* trachea. Dev. Cell *9*, 423–430.
14. Bryant, D., and Mostov, K. (2007). Development: Inflationary pressures. Nature *449*, 549–550.
15. Gürkan, C., Stagg, S.M., Lapointe, P., and Balch, W.E. (2006). The COPII cage: Unifying principles of vesicle coat assembly. Nat. Rev. Mol. Cell Biol. *7*, 727–738.
16. Ivan, V., de Voer, G., Xanthakis, D., Spoorendonk, K.M., Kondylis, V., and Rabouille, C. (2008). *Drosophila* Sec16 mediates the biogenesis of tER sites upstream of Sar1 through an arginine-rich motif. Mol. Biol. Cell *19*, 4352–4365.
17. Snapp, E.L., Iida, T., Frescas, D., Lippincott-Schwartz, J., and Lilly, M.A. (2004). The fusome mediates intercellular endoplasmic reticulum connectivity in *Drosophila* ovarian cysts. Mol. Biol. Cell *15*, 4512–4521.
18. de Navas, L., Foronda, D., Suzanne, M., and Sánchez-Herrero, E. (2006). A simple and efficient method to identify replacements of P-lacZ by P-Gal4 lines allows obtaining Gal4 insertions in the bithorax complex of *Drosophila*. Mech. Dev. *123*, 860–867.
19. Bagnat, M., Cheung, I.D., Mostov, K.E., and Stainier, D.Y. (2007). Genetic control of single lumen formation in the zebrafish gut. Nat. Cell Biol. *9*, 954–960.
20. Olver, R.E., Walters, D.V., and Wilson, S.M. (2004). Developmental regulation of lung liquid transport. Annu. Rev. Physiol. *66*, 77–101.
21. Luschnig, S., Bätz, T., Armbruster, K., and Krasnow, M.A. (2006). serpentine and vermiform encode matrix proteins with chitin binding and deacetylation domains that limit tracheal tube length in *Drosophila*. Curr. Biol. *16*, 186–194.
22. Wang, S., Jayaram, S.A., Hemphälä, J., Senti, K.A., Tsarouhas, V., Jin, H., and Samakovlis, C. (2006). Septate-junction-dependent luminal deposition of chitin deacetylases restricts tube elongation in the *Drosophila* trachea. Curr. Biol. *16*, 180–185.
23. Wu, V.M., and Beitel, G.J. (2004). A junctional problem of apical proportions: Epithelial tube-size control by septate junctions in the *Drosophila* tracheal system. Curr. Opin. Cell Biol. *16*, 493–499.
24. Hemphälä, J., Uv, A., Cantera, R., Bray, S., and Samakovlis, C. (2003). Grainy head controls apical membrane growth and tube elongation in response to Branchless/FGF signalling. Development *130*, 249–258.
25. Myat, M.M., and Andrew, D.J. (2002). Epithelial tube morphology is determined by the polarized growth and delivery of apical membrane. Cell *111*, 879–891.
26. Kerman, B.E., Cheshire, A.M., Myat, M.M., and Andrew, D.J. (2008). Ribbon modulates apical membrane during tube elongation through Crumbs and Moesin. Dev. Biol. *320*, 278–288.
27. Wodarz, A., Hinz, U., Engelbert, M., and Knust, E. (1995). Expression of crumbs confers apical character on plasma membrane domains of ectodermal epithelia of *Drosophila*. Cell *82*, 67–76.
28. Massarwa, R., Schejter, E.D., and Shilo, B.Z. (2009). Apical secretion in epithelial tubes of the *Drosophila* embryo is directed by the Formin-family protein Diaphanous. Dev. Cell *16*, 877–888.
29. Wu, G., D'Agati, V., Cai, Y., Markowitz, G., Park, J.H., Reynolds, D.M., Maeda, Y., Le, T.C., Hou, H., Jr., Kucherlapati, R., et al. (1998). Somatic inactivation of Pkd2 results in polycystic kidney disease. Cell *93*, 177–188.
30. Struhl, G., and Basler, K. (1993). Organizing activity of wingless protein in *Drosophila*. Cell *72*, 527–540.
31. Lamb, R.S., Ward, R.E., Schweizer, L., and Fehon, R.G. (1998). *Drosophila* coracle, a member of the protein 4.1 superfamily, has essential structural functions in the septate junctions and developmental functions in embryonic and adult epithelial cells. Mol. Biol. Cell *9*, 3505–3519.
32. Schonbaum, C.P., Organ, E.L., Qu, S., and Cavener, D.R. (1992). The *Drosophila melanogaster* stranded at second (sas) gene encodes a putative epidermal cell surface receptor required for larval development. Dev. Biol. *151*, 431–445.